

Conversion of a conventional superconductor into a topological superconductor by topological proximity effect

C. X. Trang¹, N. Shimamura¹, K. Nakayama^{1,2}, S. Souma^{3,4}, K. Sugawara^{1,3,4}, I. Watanabe¹, K. Yamauchi⁵, T. Oguchi⁵, K. Segawa⁶, T. Takahashi^{1,3,4}, Yoichi Ando⁷, and T. Sato^{1,3,4}

¹*Department of Physics, Tohoku University, Sendai 980-8578, Japan*

²*Precursory Research for Embryonic Science and Technology (PRESTO), Japan Science and Technology Agency (JST), Tokyo, 102-0076, Japan*

³*Center for Spintronics Research Network, Tohoku University, Sendai 980-8577, Japan*

⁴*WPI Research Center, Advanced Institute for Materials Research, Tohoku University, Sendai 980-8577, Japan*

⁵*Institute of Scientific and Industrial Research, Osaka University, Ibaraki, Osaka 567-0047, Japan*

⁶*Department of Physics, Kyoto Sangyo University, Kyoto 603-8555, Japan and*

⁷*Institute of Physics II, University of Cologne, Köln 50937, Germany*

Realization of topological superconductors (TSCs) hosting Majorana fermions is a central challenge in condensed-matter physics. One approach is to use the superconducting proximity effect (SPE) in heterostructures, where a topological insulator contacted with a superconductor hosts an effective p -wave pairing by the penetration of Cooper pairs across the interface. However, this approach suffers a difficulty in accessing the topological interface buried deep beneath the surface. Here, we propose an alternative approach to realize topological superconductivity without SPE. In a Pb(111) thin film grown on TlBiSe₂, we discover that the Dirac cone state of substrate TlBiSe₂ migrates to the top surface of Pb film and obtains an energy gap below the superconducting transition temperature of Pb. This suggests

that a BCS superconductor is converted into a TSC by the topological proximity effect. Our discovery opens a route to manipulate topological superconducting properties of materials.

Topological superconductors (TSCs) are a peculiar class of superconductors where the nontrivial topology of bulk leads to the emergence of Majorana bound states (MBSs) within the bulk superconducting gap¹⁻⁵. Since MBSs are potentially applicable to the fault-tolerant quantum computation, searching for a new type of TSCs is one of the central challenges in quantum science. A straightforward way to realize TSCs would be to synthesize an odd-parity *p*-wave superconductor; however, intrinsic *p*-wave pairing is rare in nature, as highlighted by a limited number of *p*-wave superconductor candidates hitherto reported (e.g., refs.^{6,7}). A different approach to realize TSCs is to utilize the superconducting proximity effect (SPE) in a heterostructure consisting of a conventional superconductor and a spin-orbit coupled material such as a topological insulator (TI), as initiated by the theoretical prediction of effectively *p*-wave superconductivity induced in helical Dirac fermions and Rashba states^{8,9}. This approach has been widely applied to various superconducting hybrids^{10,11,12,13,14,15,16,17}, whereas the existence of MBSs is still under intensive debates. A part of the difficulty in establishing the SPE-derived topological superconductivity may lie in the SPE process itself, since the searched MBSs are expected to be localized in the vortex core at the interface within the heterostructure, and hence are hard to be accessed by surface-sensitive spectroscopies such as scanning tunneling microscopy (STM). Therefore, it would be desirable to invent an alternative way to realize TSCs without using bulk *p*-wave superconductor or the SPE.

In this work, we present the possibility to realize TSCs by using the topological proximity effect¹⁸ (TPE); such a novel approach was discovered through our angle-resolved photoemission (ARPES) study of a heterostructure consisting of an epitaxial Pb thin film grown on a three-dimensional (3D) TI, TlBiSe₂.

Results

Fabrication and Characterization of Pb film on TlBiSe₂. The studies of SPE for generating TSCs have often employed a heterostructure consisting of a TI thin film as a top layer and a BCS superconductor as a substrate^{14,15,16,17}. On the other hand, in our TPE approach, the stacking sequence is reversed, and a superconducting Pb thin film was grown on TlBiSe₂ (Fig. 1a). We have deliberately chosen this combination, because (i) Pb films are known to maintain the superconductivity down to a few monolayers¹⁹ and (ii) TlBiSe₂ serves as a good substrate for epitaxial films¹⁸. Using the low-energy-electron-diffraction (LEED) (inset to Fig. 1d,f,h) and the ARPES results, we have estimated the in-plane lattice-constant a to be 3.5 and 4.2 Å for Pb (~20 ML) and TlBiSe₂, respectively. While the a value of Pb film is close to that of bulk²⁰, there is a sizable lattice mismatch of 19.5% between the Pb film and TlBiSe₂.

First, we discuss the overall electronic structure. As shown in Fig. 1c,d, the electronic band structure of pristine TlBiSe₂ is characterized by a Dirac-cone surface state (SS) around the $\bar{\Gamma}$ point which traverses the bulk valence and conduction bands^{21,22,23}, forming a small Fermi surface (FS) centered at $\bar{\Gamma}$. Upon evaporation of Pb on TlBiSe₂, the electronic structure drastically changes as seen in Fig. 1e,f; the holelike valence band of TlBiSe₂ disappears while several M-shaped bands emerge. The outermost holelike band crosses the Fermi level (E_F) and forms a large triangular FS (Fig. 1e). The M-shaped bands are ascribed to the quantum well states (QWSs) due to the quantum confinement

of electrons in the Pb thin film. This is supported by the experimental fact that similar M-shaped bands are also observed in a Pb(111) thin film grown on Si(111) (Fig. 1h).

The QWSs in Pb thin films with various thickness on Si(111) have been well studied by spectroscopies and calculations^{19,24,25,26,27,28}. Since the in-plane lattice constant of Pb/TlBiSe₂ is close to that of Pb/Si(111), we expect a similar electronic structure between the two. By referring to the previous studies and our band-structure calculations, we estimated the film thickness to be 17 monolayer (ML) for the case in Fig. 1e,f; see Supplementary Figure 1 and Supplementary Note 1. We observed no obvious admixture from other MLs (e.g. 16 and 18 MLs) that would create additional QWSs^{24,26}, suggesting an atomically flat nature of our Pb film. The LEED pattern of 17ML-Pb/TlBiSe₂ as sharp as that of pristine TlBiSe₂ (inset to Fig. 1f and 1d, respectively) also suggests the high crystallinity of Pb film. A careful look at Fig. 1f reveals an additional intensity spot near E_F above the topmost M-shaped band. This band is not attributed to the QWSs, and is responsible for our important finding, as described below.

Topological proximity effect. Next we clarify how the band structure of TlBiSe₂ is influenced by interfacing with a Pb film. One may expect that there is no chance to observe the band structure associated with TlBiSe₂ because the Pb film (17 ML \sim 5 nm) is much thicker than the photoelectron escape depth (\sim 0.5-1 nm). Figure 2a shows the ARPES-derived band structure near E_F obtained with a higher resolution for 17ML-Pb/TlBiSe₂, where we clearly resolve an X-shaped band above the topmost QWSs. This band resembles the Dirac-cone SS in pristine TlBiSe₂ (Fig. 2c), and is totally absent in 17ML-Pb/Si(111) (Fig. 2b), thereby ruling out the possibility of its Pb origin. The appearance of a Dirac-cone-like band in 17ML-Pb/TlBiSe₂ is surprising, because the Pb-film thickness is about ten times larger than the photoelectron escape depth. This in return

definitely rules out the possibility that the observed Dirac-cone-like band is the Dirac-cone state embedded at the Pb/TlBiSe₂ interface. Furthermore, this band is not likely to originate from the accidentally exposed SS of TlBiSe₂ through holes in Pb, since the observed bands do not involve a replica of pristine TlBiSe₂ bands and no trace of the Tl core-level peaks was found in Pb/TlBiSe₂; see Supplementary Figure 2 and Supplementary Note 2. In fact, the bulk valence band lying below 0.4 eV observed in pristine TlBiSe₂ (Fig. 2c) totally disappears in Pb/TlBiSe₂, and in addition, the Dirac point of Pb/TlBiSe₂ is shifted upward with respect to that of pristine TlBiSe₂, as clearly seen in Fig. 2d-f. These observations led us to conclude that the Dirac-cone band has migrated from TlBiSe₂ to the surface of Pb film via the TPE when interfacing Pb with TlBiSe₂ (ref.¹⁸). Such a migration can be intuitively understood in terms of the adiabatic bulk-band-gap reversal^{29,30} in the real space where the band gap (inverted gap) in TlBiSe₂ closes throughout the gapless metallic overlayer and starts to open again at the Pb-vacuum interface. It is noted that the upper branch of the Dirac-cone-like band would be connected to the quantized conduction band of the Pb film above E_F because it only crosses E_F once between Γ and M.

The band picture based on the TPE well explains the observed spectral feature in Pb/TlBiSe₂. As shown in Fig. 2g-i, the spin-degenerate topmost QWS of Pb (Fig. 2g) and the spin-polarized Dirac-cone SS of TlBiSe₂ (Fig. 2h) start to interact each other when interfacing Pb and TlBiSe₂. Due to the spin-selective band hybridization¹⁸, the Dirac-cone band is pushed upward while the QWS is pulled down (Fig. 2i). This is exactly what we see in Fig. 2a. Our systematic thickness-dependent ARPES measurements revealed a detailed hybridization behavior between the Dirac-cone band and the QWSs, supporting this scenario; see Supplementary Figure 3 and Supplementary Note 3. Noticeably, the

migration of Dirac-cone state is observed at least up to 22ML-thick (~ 6.5 nm-thick) Pb film. Such a long travel of the Dirac cone in the real space is unexpected, and hard to be reproduced by the band calculations due to large incommensurate lattice mismatch between Pb and TlBiSe₂. In fact, we have tried to calculate the band dispersion of Pb/TlBiSe₂ slab by expanding the in-plane lattice constant of Pb film to hypothetically form a commensurate system, but it caused a sizable change in the whole band structure of Pb film, resulting in the band structure totally different from the experiment. Alternatively, a calculation that uses a larger in-plane unit cell might be useful to achieve an approximate lattice match between Pb and TlBiSe₂. It is noted here that the coherency of electronic states may play an important role for the observation of a coupling with the substrate (i.e. the TPE in this study) as in the case of other quantum composite systems involving metallic overlayer³¹. We estimate the electronic coherence length in Pb film to be larger than 22 ML (~ 6.5 nm) because the topological SS is observed even in the 22ML film; see Supplementary Figure 3 and Supplementary Note 3.

Superconducting gap. The next important issue is whether the Pb/TlBiSe₂ heterostructure hosts superconductivity. To elucidate it, we first fabricated a thicker (22 ML) Pb film on TlBiSe₂ and carried out ultrahigh-resolution ARPES measurements at low temperatures. Figure 3b shows the energy distribution curve (EDC) at the \mathbf{k}_F point of the Pb-derived triangular FS (point A in Fig. 3a) measured at $T = 4$ and 10 K across the superconducting transition temperature T_c of bulk Pb (7.2 K). At $T = 4$ K, one can clearly recognize a leading-edge shift toward higher E_B together with a pile up in the spectral weight, a typical signature of the superconducting-gap opening. This coherence peak vanishes at $T = 10$ K due to the gap closure, as better visualized in the symmetrized EDC (Fig. 3c). We have estimated the superconducting-gap size at $T = 4$ K to be 1.3 meV from

the numerical fittings. This value is close to that of bulk Pb (~ 1.2 meV) (ref.³²), suggesting that the T_c is comparable to that of bulk Pb.

Since the superconductivity shows up on the Pb film, we now address an essential question whether the migrating Dirac-cone band hosts superconductivity. We show in Fig. 3d-i the EDCs and corresponding symmetrized EDCs at $T = 4$ and 10 K for the 17 ML sample measured at three representative \mathbf{k}_F points (points A-C in Fig. 3a). At point A on the Pb-derived FS, we observe the superconducting-gap opening (Fig. 3d), similarly to the 22 ML film. At point B (C) where the migrating Dirac-cone band crosses E_F along the $\overline{\Gamma K}$ ($\overline{\Gamma M}$) line, we still observe a gap as seen in Fig. 3f (Fig. 3h). This indicates that an isotropic superconducting gap opens on the migrating Dirac-cone FS. We observed that this gap persists at least down to 12 ML, confirming that the superconducting gap is not an artifact which accidentally appears at some specific film thickness; see Supplementary Figure 4 and Supplementary Note 4. We have also confirmed that the gap-opening is not an inherent nature of the original topological SS in pristine TlBiSe₂, by observing no leading-edge shift or spectral-weight suppression at E_F at 4 K in pristine TlBiSe₂ (Fig. 3j,k).

Discussion

The present results show that the superconducting gap opens on the entire FS originating from both the Pb-derived QWSs and the migrating Dirac-cone band (Fig. 3l). The emergence of an isotropic superconducting gap on the Dirac-cone FS suggests that the 2D topological superconductivity is likely to be realized, since this heterostructure satisfies the theoretically proposed condition for the effectively p -wave superconducting helical-fermion state⁸. In this regard, one may think that such realization is a natural consequence of making heterojunction between superconductor and TI. However, the

present study proposes an essentially new strategy to realize the 2D topological superconductivity. In the ordinary approach based on the SPE (Fig. 3m), the topological Dirac-cone state hosts the effective p -wave pairing at the interface due to the penetration of Cooper pairs from the superconductor to the TI. On the other hand, the present approach does not rely on this phenomenon at all, because the topological Dirac-cone state appears on the top surface of a superconductor (Fig. 3n) via the TPE.

One can view this effect as a conversion of a conventional superconductor (Pb film without topological SS) to a TSC (Pb film with topological SS) by interfacing. The present approach to realize 2D TSCs has an advantage in the sense that the pairing in the helical-fermion state (and the MBS as well) is directly accessed by surface spectroscopies such as STM and ARPES. The superconducting helical fermions would be otherwise embedded deep at the interface and are hard to be accessed if the TPE does not occur. Moreover, the observed gap magnitude on the topological SS is comparable to that of the original Pb, unlike the SPE-induced gap which is usually smaller. This result tells us that the so-far overlooked TPE had better be seriously taken into account in many superconductor-TI hybrids. Also, the present study points to the possibility of realizing even wider varieties of 2D TSCs by using the TPE. It is noted that the topological states in Pb/TlBiSe₂ are electrically shorted out by the metallic QWSs, unlike the case of some TI films on top of superconductors. This needs to be considered in the application because single conducting channel from the Dirac-cone states would be more preferable. In this regard, the present approach utilizing the TPE and the existing approach using the SPE would be complementary to each other.

Methods

Sample preparation. High-quality single crystals of TlBiSe₂ were grown by a modified Bridgman method²¹. To prepare a Pb film, we first cleaved a TlBiSe₂ crystal under ultrahigh vacuum with scotch tape to obtain a shiny mirror-like surface, and then deposited Pb atoms (Purity; 5N) on the TlBiSe₂ substrate using the molecular-beam epitaxy technique while keeping the substrate temperature at $T = 85$ K. A Pb(111) film on Si(111), used as a reference, was fabricated by keeping the same substrate temperature. The film thickness was controlled by the deposition time at a constant deposition rate. The actual thickness was estimated by a comparison of ARPES-derived band dispersions with the band-structure calculations for free-standing multilayer Pb.

ARPES measurements. ARPES measurements were performed with the MBS-A1 electron analyzer equipped with a high-intensity He discharge lamp. After the growth of Pb thin film by evaporation, it was immediately transferred to the sample cryostat kept at $T = 30$ K in the ARPES chamber, to avoid the clusterization of Pb which is accelerated at room temperature (note that such clusterization hinders the detailed investigation of the surface morphology by atomic-force microscopy). We used the He-I α resonance line ($h\nu = 21.218$ eV) to excite photoelectrons. The energy resolution of ARPES measurements was set to be 2-40 meV. The sample temperature was kept at $T = 30$ K during the ARPES-intensity-mapping measurements, while $T = 4$ and 10 K for the superconducting-gap measurements. The Fermi level (E_F) of the samples was referenced to that of a gold film evaporated onto the sample holder.

Band calculations: First-principles band-structure calculations were carried out by a projector augmented wave method implemented in Vienna Ab initio Simulation Package (VASP) code³³ with generalized gradient approximation (GGA) potential³⁴. After the

crystal structure was fully optimized, the spin-orbit coupling was included self-consistently.

Data availability

The data sets generated/analyzed during the current study are available from the corresponding author on reasonable request.

References

1. Hasan, M. Z. & Kane, C. L. Colloquium: Topological insulators. *Rev. Mod. Phys.* **82**, 3045–3067 (2010).
2. Qi, X. L. & Zhang, S. C. Topological insulators and superconductors. *Rev. Mod. Phys.* **83**, 1057-1110 (2011).
3. Ando, Y. & Sato, M. Topological superconductors: a review. *Rep. Prog. Phys.* **80**, 076501 (2017).
4. Alicea, J. New directions in the pursuit of Majorana fermions in solid state systems. *Rep. Prog. Phys.* **75**, 076501 (2012).
5. Beenakker, C. W. J. Search for Majorana Fermions in Superconductors. *Annu. Rev. Condens. Matter Phys.* **4**, 113 (2013).
6. Maeno, Y. et al. Superconductivity in a layered perovskite without copper. *Nature (London)* **372**, 532-534 (1994).
7. Hor, Y. S. et al. Superconductivity in $\text{Cu}_x\text{Bi}_2\text{Se}_3$ and its implications for pairing in the undoped topological insulator. *Phys. Rev. Lett.* **104**, 057001 (2010).
8. Fu, L. & Kane, C. L. Superconducting proximity effect and Majorana fermions at the surface of a topological insulator. *Phys. Rev. Lett.* **100**, 096407 (2008).
9. Sato, M. & Fujimoto, S. Topological phases of noncentrosymmetric superconductors: Edge states, Majorana fermions, and non-Abelian statistics. *Phys. Rev. B* **79**, 094504 (2009).
10. Mourik, V. et al. Signatures of Majorana fermions in hybrid superconductor-semiconductor nanowire devices. *Science* **336**, 1003-1007 (2012).

11. Das, A. et al. Zero-bias peaks and splitting in an Al-InAs nanowire topological superconductor as a signature of Majorana fermions. *Nat. Phys.* **8**, 887–895 (2012).
12. Deng, M. T. et al. Majorana bound state in a coupled quantum-dot hybrid-nanowire system. *Science* **354**, 1557–1562 (2016).
13. Nadj-Perge, S. et al. Observation of Majorana fermions in ferromagnetic atomic chains on a superconductor. *Science* **346**, 602–607 (2014).
14. Wang, M. et al. The coexistence of superconductivity and topological order in the Bi₂Se₃ thin films. *Science* **336**, 52-55 (2012).
15. Xu, S.-Y. et al. Momentum-space imaging of Cooper pairing in a half-Dirac-gas topological superconductor. *Nat. Phys.* **10**, 943–950 (2014).
16. Sun, H. -H. et al. Coexistence of topological edge state and superconductivity in bismuth ultrathin film. *Nano Lett.* **17**, 3035–3039 (2017).
17. Flötotto, D. et al. Superconducting pairing of topological surface states in bismuth selenide films on niobium. *Science Adv.* **4**, eaar7214 (2018).
18. Shoman, T. et al. Y. Topological proximity effect in a topological insulator hybrid. *Nat. Comm.* **6**, 6547 (2015).
19. Qin, S., Kim, J. & Shih, C.-K. Superconductivity at the two-dimensional limit. *Science* **324**, 1314-1317 (2009).
20. Davey, W. P. Precision measurements of the lattice constants of twelve common metals. *Phys. Rev.* **25**, 753 (1925).
21. Sato, T. et al. Direct evidence for the Dirac-cone topological surface states in the ternary chalcogenide TlBiSe₂. *Phys. Rev. Lett.* **105**, 136802 (2010).
22. Kuroda, K. et al. Experimental realization of a three-dimensional topological insulator phase in ternary chalcogenide TlBiSe₂. *Phys. Rev. Lett.* **105**, 146801 (2010).
23. Chen, Y. L. et al. Single Dirac cone topological surface state and unusual thermoelectric property of compounds from a new topological insulator family. *Phys. Rev. Lett.* **105**, 266401 (2010).
24. Wei, C. M. & Chou, M. Y. Theory of quantum size effects in thin Pb(111) films. *Phys. Rev. B* **66**, 233408 (2002).

25. Man, A., Dil, J. H., Ettema, A. R. H. F. & Weitering, H. H. Quantum electronic stability and spectroscopy of ultrathin Pb films on Si(111)7×7. *Phys. Rev. B* **66**, 195410 (2002).
26. Upton, M. H., Miller, T., & Chiang, T.-C. Absolute determination of film thickness from photoemission: Application to atomically uniform films of Pb on Si. *Appl. Phys. Lett.* **85**, 1235 (2004).
27. Upton, M. H., Wei, C. W., Chou, M. Y., Miller, T., & Chiang, T.-C. Thermal stability and electronic structure of atomically uniform Pb films on Si(111). *Phys. Rev. Lett.* **93**, 026802 (2004).
28. Zhang, Y.-F. et al. Band structure and oscillatory electron-phonon coupling of Pb thin films determined by atomic-layer-resolved quantum-well states. *Phys. Rev. Lett.* **95**, 096802 (2005).
29. Wang, X., Bian, G., Miller, T., & Chiang, T.-C. Topological spin-polarized electron layer above the surface of Ca-terminated Bi₂Se₃. *Phys. Rev. B* **87**, 035109 (2013).
30. Wang, X., Bian, G., Miller, T., & Chiang, T.-C. Topological quantum well resonances in metal overlayers. *Phys. Rev. B* **87**, 235113 (2013).
31. Liu, Y. et al. Interface-induced complex electronic interference structures in Ag films on Ge(111). *Phys. Rev. B* **78**, 035443 (2008).
32. Chainani, A., Yokoya, T., Kiss, T. & Shin, S. Photoemission spectroscopy of the strong-coupling superconducting transitions in lead and niobium. *Phys. Rev. Lett.* **85**, 1966 (2000).
33. Kresse, G. & Furthmüller, J. Efficient iterative schemes for *ab-initio* total energy calculations using a plane-wave basis set. *Phys. Rev. B* **54**, 11169–11186 (1996).
34. Perdew, J. P., Burke, K. & Ernzerhof, M. Generalized gradient approximation made simple. *Phys. Rev. Lett.* **77**, 3865-3868 (1996).

Acknowledgements

We thank T. Nakamura, K. Hori, A. Tokuyama, and T. Ren for their assistance in the ARPES experiments. This work was supported by Grant-in-Aid for Scientific Research on Innovative Areas "Topological Materials Science" (JSPS KAKENHI Grant Number JP15H05853, No. JP18H04227, and No. JP15K21717), JST-CREST (No. JPMJCR18T1), JST-PRESTO (No. JPMJPR18L7), and Grant-in-Aid for Scientific Research (JSPS KAKENHI Grant Numbers JP17H01139, JP15H02105, JP26287071, and JP25287079). The work in Cologne was funded by the Deutsche Forschungsgemeinschaft (DFG, German Research Foundation) - Project number 277146847 - CRC 1238 (Subproject A04).

Author Contributions

The work was planned and proceeded by discussion among C.X.T., K.N., S.S., K. Sugawara, T.S., T.T. and Y.A. K. Segawa carried out the growth of bulk single crystals and their characterization. C.X.T and I.W. fabricated ultrathin films. C.X.T. N.S. and I.W. performed the ARPES measurements. K.Y. and T.O. carried out the band calculations. C.X.T. and T.S. finalized the manuscript with inputs from all the authors.

Additional information

Supplementary Information accompanies this paper at <http://..>

Competing Interests: The authors declare no competing interests.

Correspondence and requests for materials should be addressed to T. Sato (e-mail: t-sato@arpes.phys.tohoku.ac.jp).

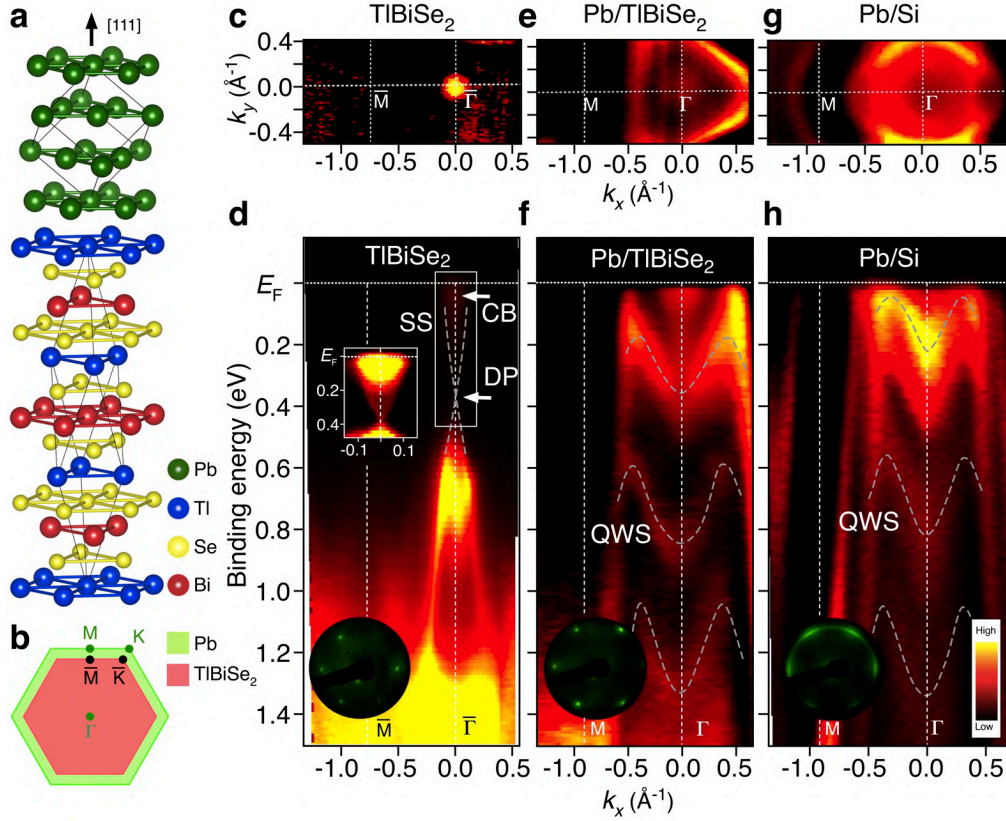


Fig. 1 Crystal and electronic structures of Pb(111) thin film on TlBiSe₂. **a** Heterostructure consisting of Pb and TlBiSe₂. **b** Comparison of Brillouin zone between TlBiSe₂ (red) and Pb (green). **c** Plot of ARPES intensity at E_F as a function of in-plane wave vector (namely, Fermi surface) around the $\overline{\Gamma M}$ line for pristine TlBiSe₂, measured with the He-I α line ($h\nu = 21.218$ eV). **d** ARPES-derived band structure along the $\overline{\Gamma M}$ cut for pristine TlBiSe₂. Inset shows the ARPES intensity with enhanced color contrast in the area enclosed by white rectangle. **e, f** Same as (c, d) but for 17ML-Pb/TlBiSe₂. **g, h** Same as (e, f) but for 17ML-Pb/Si(111). SS, CB, DP, and QWS denote the surface state, conduction band, Dirac point, and quantum well state, respectively. Arrows in (d) indicate the location of CB and DP. Dashed gray curves are a guide for the eyes to trace the SS and QWSs. Insets to (d, f) and (h) are the LEED patterns of the respective films

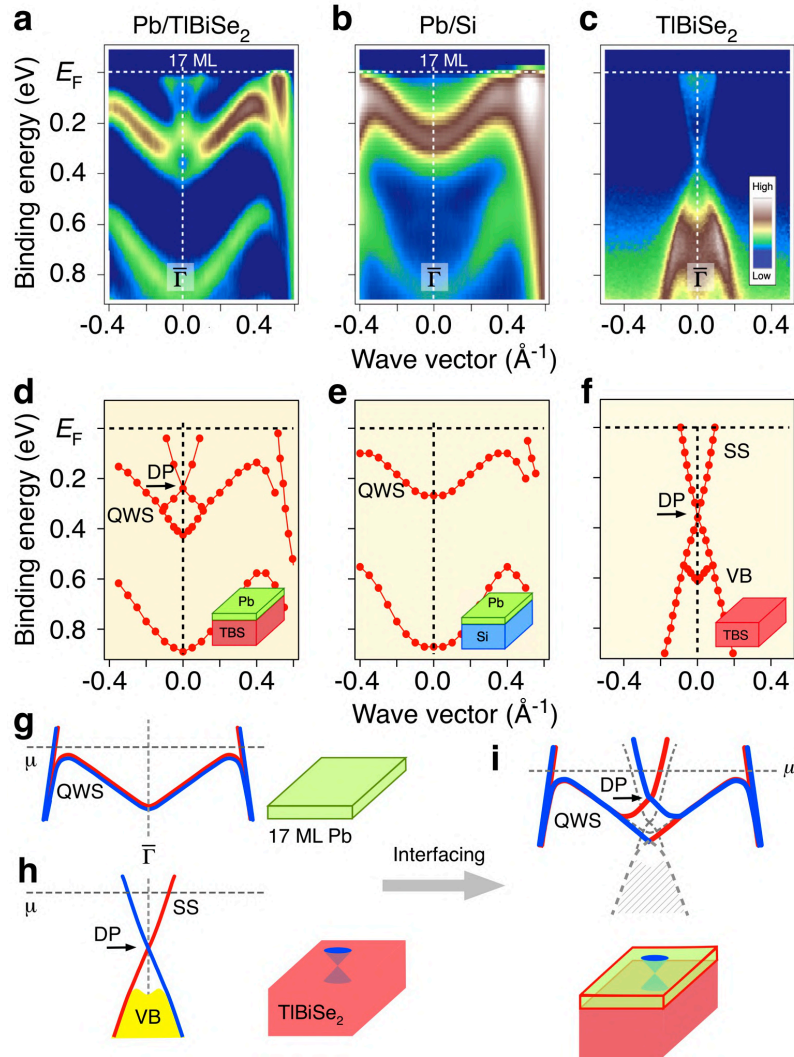


Fig. 2 Migration of topological surface states to the surface of Pb film. **a-c** ARPES-derived band-structure near E_F around the $\bar{\Gamma}$ point for 17ML-Pb/TlBiSe₂, 17ML-Pb/Si(111), and pristine TlBiSe₂, respectively, with the He-I α line. The data were obtained along the $\bar{\Gamma}\bar{K}$ cut parallel to the analyzer slit, so that the energy and momentum resolutions are better than the data in Fig. 1d,f,h measured along the $\bar{\Gamma}\bar{M}$ cut perpendicular to the analyzer slit. **d-f** Experimental band dispersions extracted from the peak positions of MDCs/EDCs for (a-c). **g-i** Schematics of the hybridization between topological Dirac-cone state and QWSs, showing the migration of topological Dirac-cone state upon interfacing Pb with TlBiSe₂. Dashed curves in Fig. 2i indicate the band dispersion without hybridization. Note that the bulk VB of TlBiSe₂ indicated by gray shade becomes invisible on the Pb/TlBiSe₂ interface, because only the topological SS migrates to the top surface

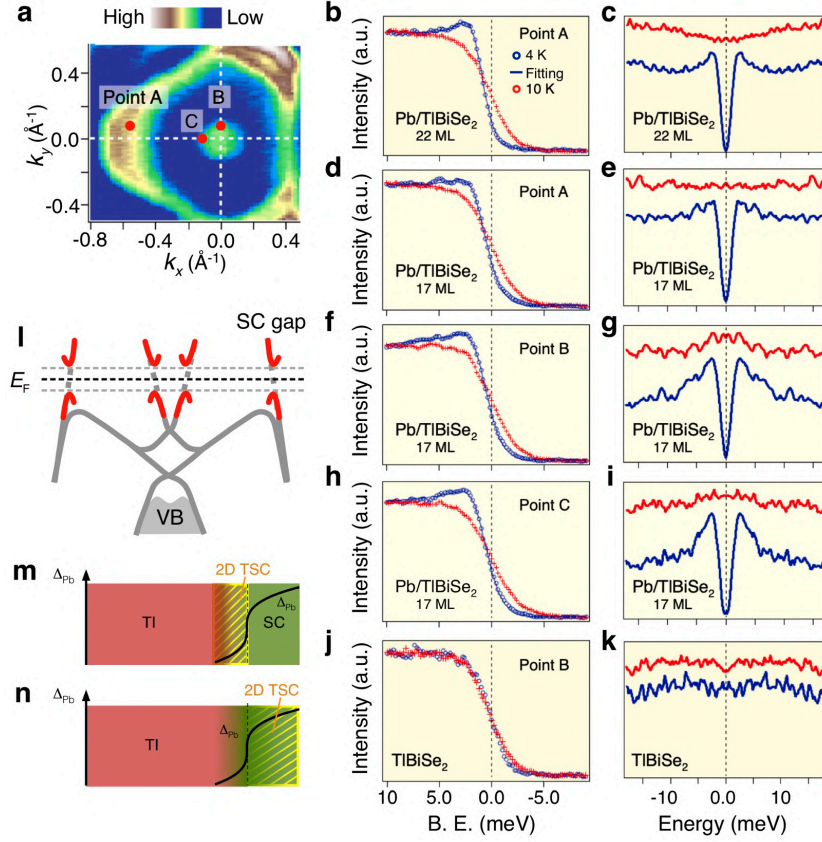
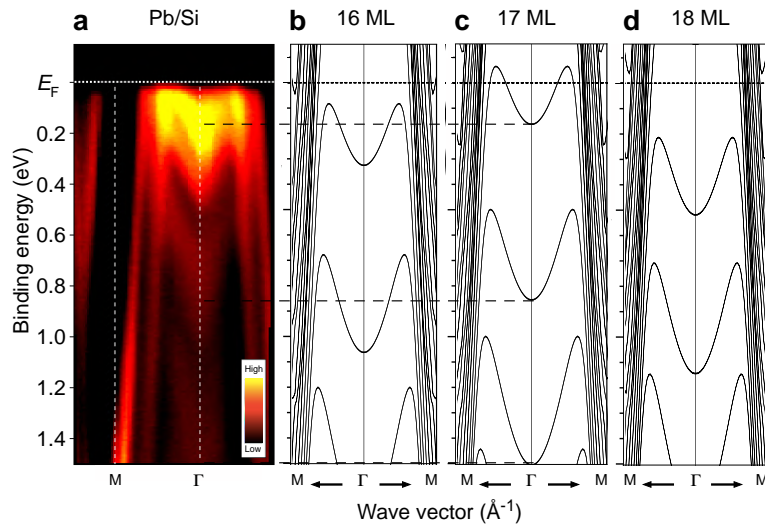
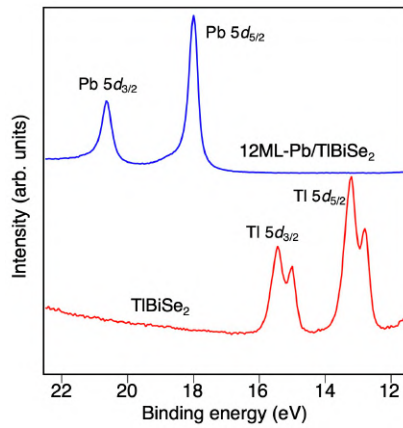


Fig. 3 Possible topological superconductivity in Pb film. **a** ARPES intensity mapping at E_F for 22ML-Pb/TlBiSe₂. **b, c** Ultrahigh-resolution EDCs and corresponding symmetrized EDCs, respectively, at $T = 4$ K and 10 K, measured at point A in **(a)** (k_F point of the QWS) for 22ML-Pb/TlBiSe₂. **d, e** Same as **(b, c)**, respectively, but for 17ML-Pb/TlBiSe₂. **f, g** Same as **(d, e)**, respectively, but measured at point B (k_F point of the topological SS). **h, i** Same as **(d, e)**, respectively, but measured at point C. **j, k** Same as **(f, g)**, respectively, but for pristine TlBiSe₂. Blue solid curve in the EDC at $T = 4$ K in **(b, d, f, h)** is the result of numerical fittings using the Dynes function multiplied by the Fermi-Dirac distribution function, convoluted with a resolution function. **l** Illustration of the superconducting-gap opening on the QWS- and TSS-derived bands. **m** Conventional view on the realization of 2D TSC via SPE. **n** Proposed method to realize 2D TSC by converting a conventional superconductor into a TSC through the TPE

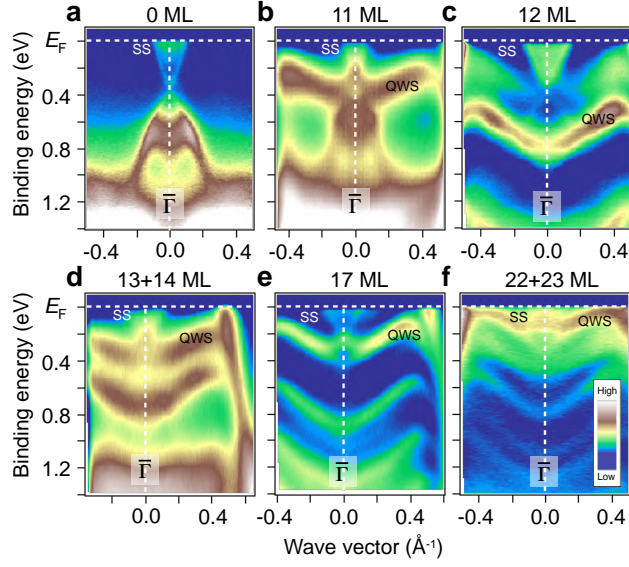
SUPPLEMENTARY INFORMATION for
Conversion of a conventional superconductor into a topological
superconductor by topological proximity effect
Trang et al.



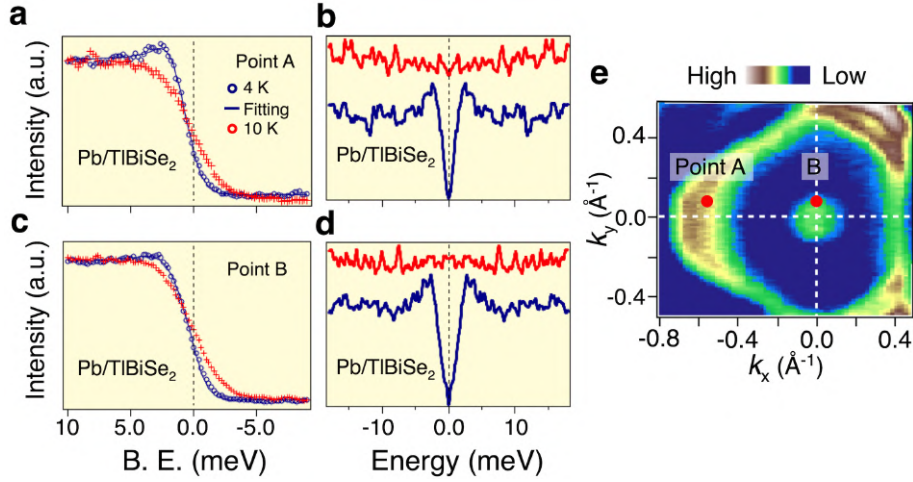
Supplementary Figure 1. Comparison of band dispersion of Pb between ARPES and band calculations. **a** Plot of ARPES intensity measured along the $\overline{\Gamma M}$ cut for 17 ML Pb film on Si(111). **b-d** Calculated band structures along the $\overline{\Gamma M}$ cut for 16, 17, and 18 MLs of Pb slabs, respectively.



Supplementary Figure 2. Comparison of ARPES spectrum around the Tl $5d$ and Pb $5d$ core-level region between pristine TlBiSe₂ and 12ML-Pb/TlBiSe₂ measured with the He II α photons ($h\nu = 40.8$ eV).



Supplementary Figure 3. Film-thickness dependence of experimental band structure in Pb/TlBiSe₂. **a-f** Plots of ARPES intensity of Pb(111)/TlBiSe₂ measured along the $\bar{\Gamma}\bar{K}$ cut for various film thickness n ($n = 0, 11, 12, 13+14$, and $22+23$ ML, respectively). $13+14$ ML represents the spatially inhomogeneous Pb film in which 13-ML and 14-ML islands are formed on TlBiSe₂.



Supplementary Figure 4. Observation of superconducting gap in 12ML Pb/TlBiSe₂. **a, b** Ultrahigh-resolution EDCs and corresponding symmetrized EDCs, respectively, at $T = 4$ K and 10 K measured at point A on the Fermi surface shown in **e**, for 12 ML Pb film on TlBiSe₂. **c, d** Same as (a, b), respectively, but measured at point B in (e). **e** Mapping of ARPES intensity near E_F and measured \mathbf{k}_F points (points A and B).

Supplementary Note 1: Estimation of the film thickness using the band-structure calculations

We have estimated the number of monolayers (MLs) of Pb films by comparing the energy location of the quantum well states (QWSs) between the ARPES results and the slab calculations for free-standing n -ML Pb film ($n = 10-24$). Supplementary Figure 1 shows a comparison of band structure along the $\overline{\Gamma M}$ cut between the ARPES result for a 17 ML Pb film on Si(111) and corresponding band structures calculated for free-standing 16-18ML films. Both the ARPES and the calculations commonly show a M-shaped feature, suggesting that this feature originates from the QWSs of Pb film. The energy location of the QWSs in the experiment for a 17 ML Pb film shows a reasonable agreement with that of the calculation for 17 ML (Supplementary Figure 1c), whereas the calculations for 16 or 18 ML show a deviation from the ARPES result. This suggests that our way of estimating the film thickness has an accuracy within 1 ML. We have applied the same method for all Pb films fabricated on TlBiSe₂ or Si(111) to estimate the film thickness. We confirmed that the estimated film thickness is consistent with that estimated from the Pb-deposition time/rate during the molecular-beam epitaxy. It is noted that there exists a small quantitative difference in the energy position of QWSs between the slab calculations and the ARPES results (e.g., ~ 50 meV at the Γ point for the second QWSs). This may be understood in terms of the substrate effect related to the interfacial phase shifts.

Supplementary Note 2: Change in the core-level peaks upon evaporation of Pb on TlBiSe₂

We measured the ARPES spectrum in a wide energy region covering the Tl 5*d* and Pb 5*d* core-level region before/after evaporation of Pb on TlBiSe₂. As shown in Supplementary Figure 2, the Tl 5*d* core-level peaks located at the binding energy E_B of $\sim 12-16$ eV completely disappear after depositing a 12ML Pb film on TlBiSe₂, while the Pb 5*d* core-level peaks simultaneously evolve at $\sim 17.5-21$ eV. This suggests that the surface measured by ARPES is fully covered with Pb, and the observed Dirac-cone feature in Pb/TlBiSe₂ indeed migrates from the surface of TlBiSe₂. Absence of Tl peak

after the evaporation of Pb might suggest a clean interface/surface nature, whereas a possibility of Se segregation is not completely excluded since the energy range of the measurement does not cover Se core levels.

Supplementary Note 3: Thickness dependence of the band structure of Pb thin films on TlBiSe₂

We observed the Dirac-cone energy band hybridized with the QWSs in the Pb thin film on TlBiSe₂ over a wide range of film thickness ($n = 11-22$ ML). We show in Supplementary Figure 3 the film-thickness dependence of ARPES intensity measured along the $\overline{\Gamma K}$ cut. One can clearly recognize the QWSs whose energy position systematically changes on increasing the number of layers n . One can also identify an additional feature above the topmost QWSs, which is assigned to the Dirac-cone band migrating from the TlBiSe₂ surface. We found that the energy location of the Dirac-cone band, as well as its sharpness and intensity, systematically changes with the film thickness. Moreover, the Dirac-cone band looks as if it is heavily hybridized with the topmost QWSs, producing a complicated intensity profile around the intersection of the Dirac-cone band and the QWSs.

Supplementary Note 4: Superconducting-gap measurement for the 12 ML Pb thin film

We observed a superconducting gap in the Pb thin film on TlBiSe₂ at least down to the film thickness of 12 ML. Supplementary Figure 4a-d shows the EDCs and symmetrized EDCs at two representative Fermi wave vectors (\mathbf{k}_F) on the Pb-derived triangular Fermi surface and the Dirac-cone band migrating from TlBiSe₂ (points A and B in Supplementary Figure 4e, respectively) measured at $T = 4$ and 10 K. Similarly to 17ML-Pb/TlBiSe₂ (Fig. 3d-i in the text), we observe a small pile up in the spectral weight accompanied with a leading-edge shift for both points, indicative of the superconducting-gap opening. We confirmed that this spectral change is due to the superconducting-gap opening, since such spectral feature is absent at $T = 10$ K above T_c of bulk Pb (7.2 K). We

have estimated the magnitude of superconducting gap to be 1.2 ± 0.1 meV for both \mathbf{k}_F points by the numerical fittings using the Dynes function multiplied by the Fermi-Dirac distribution convoluted with a resolution function. This value is similar to those estimated for the 17 and 22 ML films, suggesting that the T_c value of our Pb films maintains the constant value similar to bulk Pb at least down to 12 ML.

We found that the coherence peak in the 22 ML film (Fig. 3b in the text) is better seen than the 17 ML (Fig. 3d in the text) and 12 ML (Supplementary Figure 4a,b) films. This is also reflected in the broadening factor (damping parameter Γ) in the numerical fittings with Dynes function at point A on the Pb-derived Fermi surface (0.2, 0.8, and 0.5 meV for the 22-, 17-, and 12-ML films, respectively). While we do not know an exact origin for such a difference, we speculate that the surface quality, such as inhomogeneity and domain size of Pb film, is somehow related to the quasiparticle scattering rate. This conjecture could be further examined by elucidating the relationship between the surface structure and the superconducting gap with low-temperature scanning tunneling microscopy.